Universitat Politècnica de Catalunya (UPC)
Universitat Autònoma de Barcelona (UAB)
Universitat de Barcelona (UB)
Institut de Ciències Fotòniques (ICFO)

http://www.photonicsbcn.eu

Master in Photonics

MASTER THESIS WORK

Quantum photon correlations at the single-atom level in free space

Daniel Goncalves Romeu

Supervised by Prof. Darrick Chang (ICFO) and Dr. Mariona Moreno Cardoner (UAB, ICFO)

Presented on date 31th August 2019

Registered at

Escola Tècnica Superior d'Enginyeria de Telecomunicació de Barcelona

Quantum photon correlations at the single-atom level in free space

Daniel Goncalves Romeu

ICFO-Institut de Ciencies Fotoniques, The Barcelona Institute of Science and Technology, Barcelona, Spain.

E-mail: daniel.goncalves@icfo.eu

Abstract. In this project, we present a novel approach to calculate and engineer the photon correlations emerging from the interference between an input field and the field scattered by an atom in free space. Historically, it has been difficult to observe robust quantum correlations in the total field, as the inefficient atom-light coupling in free space usually causes the scattered field to be small in comparison to the input. To overcome this issue, we propose the use of separate pump and probe beams, where the former effectively enhances the atomic emission to be comparable to the probe. Additionally, we elucidate the physical origin of the non-classical correlations predicted, by studying the transient atomic state after the measurement of a photon.

1. Introduction and motivation

One of the main purposes of quantum optics is to describe the phenomena resulting from the interaction between atoms and photons [1]. At the same time, promising applications of quantum physics like quantum information or computation rely on being able to control and tune this interaction [2, 3]. To observe these quantum phenomena, one needs a strong coupling between light and matter. Nowadays, this can be obtained with a handful of different approaches: high finesse cavities [4, 5], large atomic ensembles [6] or optical wave-guides [7], among others. In the case of a single atom in free space, the usual approach is to use diffraction-limited focusing, motivated by the fact that the absorption cross-section of an atom is on the order of the wavelength squared [8].

However, such tight focusing is not easy to obtain. The atom-light coupling is inefficient under standard laboratory conditions, where optics with low numerical apertures (NA<0.9) are typically used [9]. Even so, larger focusing with a single beam increases the coupling to moderate strength, not enough for some applications. An enhancement of this method consists in using techniques to deal with the diffraction limit, such as the 4π illumination [10], obtaining a stronger light-matter interaction.

In this work, we would like to explore a different approach to observe quantum optical effects at the single-atom level. Among all the possible phenomena to discuss, we study the quantum photon correlations emerging from the interference between an input field and the field scattered by an atom in free space.

1.1. Photon correlations with single atoms

As seen by S. J. Van Enk and H. J. Kimble [11], non-trivial photon correlations emerge from the interaction between an ideal two-level atom and an input coherent field. These include extremely large photon bunching, $g^{(2)}(0,\mathbf{r}) \to \infty$, and total photon anti-bunching, $g^{(2)}(0,\mathbf{r}) \to 0$. It is possible to prove that these phenomena only occur when two conditions are met. First, the input and scattered fields must have similar amplitudes. Depending on the amplitude ratio, one has photon bunching ($E_{in}/E_{atom} = 1$) or anti-bunching ($E_{in}/E_{atom} = 1/2$). Second, the superposition has to be destructive, meaning that input and scattered fields must have opposite phases. In Figure 1, we simulate the $g^{(2)}(0,\mathbf{r})$ at each point of the plane (y,+z) obtained from the superposition between a paraxial, Gaussian beam with waist $w_0 = 5\lambda$, propagating along $\mathbf{z}$ and polarization $\mathbf{x}$; with the field scattered by a two-level atom. We see two narrow lines at $y \approx \pm 10\lambda$ with the non-trivial total bunching and anti-bunching.

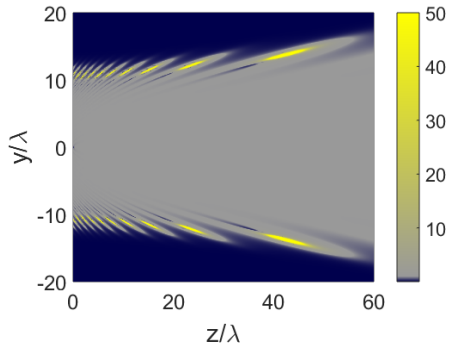

Figure 1: Total field correlations expressed through the $g^{(2)}(0,\mathbf{r})$ for a paraxial, Gaussian input beam with waist $w_0 = 5\lambda$. The atom is placed at (0,0). Color code: yellow for bunching and blue for anti-bunching. Data truncated at $g^{(2)} \leq 50$.

The follow up question is whether this is measurable or not. A point-like measurement of the fields to obtain $g^{(2)}(0,\mathbf{r})$ is not feasible from the experimental standpoint: we need to collect the fields with lenses. Extrapolating the conditions from the point-like case, we hypothesize that the collected input field must be comparable to the scattered one to see these effects. However, the scattered field is much weaker than the input one due to inefficient light-atom coupling. Without requiring a diffraction-limited focusing, we propose the following approach to increase the power of the scattered field. We illuminate the atom with two beams (called pump and probe) in perpendicular directions. We measure the $g^{(2)}(0)$ of field collected at the probe lens, which contains the probe and the scattered field. The pump is added to enhance the atomic dipole, effectively increasing the scattered field, and is not collected at the lens of interest. A setup allowing all of the above could be a Maltese cross-illumination configuration, where four aspheric, high-NA lenses are placed as in Figure 2 [12] such that the pump and probe only cross at the position of the atom. Then, our physical system will consist of a two-level atom and three fields: pump, probe and scattered.

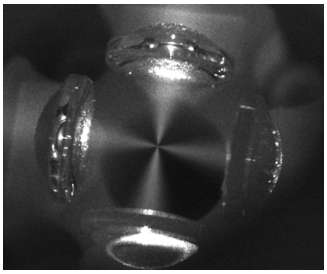

Figure 2: Maltese cross setup.

The aim of this project is to study if relevant effects in the $g^{(2)}(0)$ can be observed when collecting the light in the aforementioned conditions. To do so, first we will introduce the theoretical framework. Afterwards, we will discuss how the photon measurements are done and we will study the quantum photon correlations.

2. Theoretical framework

This section provides a brief introduction to some results and definitions needed for the following sections. We start addressing the quantum dynamics of the single-atom within the density matrix formalism. After that, we define the concept of mode projection.

2.1. Quantum description of the atomic state

The full dynamics of the light emission and re-scattering by a neutral atom in free-space can be related to an effective model containing only atomic degrees of freedom and the incident fields [13, 14]. Within this framework, the atom has ground state $|g\rangle$ and excited state $|e\rangle$, as well as a dipolar transition moment $\mathbf{d}_{eg}$ (assumed to be along $\hat{\mathbf{x}}$) coupled to a free space optical mode. The effective dynamics for the atomic density matrix $\hat{\rho}$ are described by the master equation

$$\dot{\hat{\rho}} = -i[\hat{H}, \hat{\rho}] + \mathcal{L}[\hat{\rho}] = -i[\hat{H}, \hat{\rho}] + \frac{\Gamma_0}{2}\left(2\hat{\sigma}^{ge}\hat{\rho}\hat{\sigma}^{eg} - \hat{\sigma}^{ee}\hat{\rho} - \hat{\rho}\hat{\sigma}^{ee}\right), \tag{1}$$

where Γ_0 is the decay rate in vacuum and $\hat{\sigma}^{ij}$ are the atomic coherence operators $|i\rangle\langle j|$ with $\{i, j\} \in \{e, g\}$. The Hamiltonian from Eq. (1) contains a free energy term and a light-atom interaction term. In the rotating frame, it has the form

$$\hat{H} = -\hbar\Delta\ \hat{\sigma}^{ee} - \hbar\left(\frac{\Omega}{2}\hat{\sigma}^{eg} + h.c.\right), \tag{2}$$

where $\Delta = \omega - \omega_0$ is the detuning of the field at frequency ω with respect to the transition frequency ω_0 and $\Omega = \mathbf{E}^{in} \cdot \mathbf{d}^{eg}/\hbar$ is the Rabi frequency, which in general can be complex. The steady state solutions of Eq. (1) for the excited state population ρ_{ee} and the coherence ρ_{eg} are [15]

$$\rho^{ee}_{(t\to\infty)} = \frac{|\Omega|^2}{\Gamma_0^2}\frac{1}{1 + \left(\frac{2\Delta}{\Gamma_0}\right)^2 + 2\frac{|\Omega|^2}{\Gamma_0^2}}, \qquad \rho^{eg}_{(t\to\infty)} = \frac{i\Omega}{\Gamma_0}\frac{1 + i2\Delta/\Gamma_0}{1 + \left(\frac{2\Delta}{\Gamma_0}\right)^2 + 2\frac{|\Omega|^2}{\Gamma_0^2}}. \tag{3}$$

Throughout this work, we will be interested in the resonant, weak driving regime, where $\Omega \ll \Gamma_0$ and $\Delta = 0$. The steady state solutions under these conditions take the form $\rho_{ee} \to |\Omega|^2/\Gamma_0^2$ for the excited state population and $\rho_{eg} \to i\Omega/\Gamma_0$ for the coherence. Now we define the concept of mode projection.

2.2. Mode projecting measurements and fields

Let us start from the quantization of the electromagnetic field. Here we will outline the main results obtained from the full derivation in Appendix A. One can decompose any field operator in terms of quantized plane-wave modes with a specific wave vector $\mathbf{k}$ and polarization $\hat{\epsilon}_{\mathbf{k},j}$ [16]. Each mode has associated bosonic annihilation and creation operators, with the usual conjugation relations. In the Schrodinger picture, we have

$$\hat{\mathbf{E}}(\mathbf{r}) = \sum_{\mathbf{k}}\sum_{\hat{\epsilon}_{k,j}} E_0(k)\left[\hat{a}_{\mathbf{k},\hat{\epsilon}_{k,j}} e^{-i\mathbf{k}\cdot\mathbf{r}} + \hat{a}^{\dagger}_{\mathbf{k},\hat{\epsilon}_{k,j}} e^{i\mathbf{k}\cdot\mathbf{r}}\right]\hat{\epsilon}_{\mathbf{k},j}\ , \tag{4}$$

where $E_0(k) = [\hbar\omega_k/(2V\epsilon_0)]^{1/2}$ is a normalization constant for the Hamiltonian to be in the right units. Next, we split Eq. (4) into a positive and negative frequency parts. We change our notation such that the positive frequency part is $\hat{\mathbf{E}}$, with the annihilation operators, and the negative frequency part is $\hat{\mathbf{E}}^\dagger$, with the creation ones. The positive part of each mode in Eq. (4) has the form $\hat{\mathbf{E}}_{\mathbf{k},\hat{\epsilon}_{k,j}}(\mathbf{r},t) = E_0(k)\mathbf{u}_{\mathbf{k},\hat{\epsilon}_{k,j}}(r,t)\hat{a}_{\mathbf{k},\hat{\epsilon}_{k,j}}$, where $\mathbf{u}_{\mathbf{k},\hat{\epsilon}_{k,j}}(\mathbf{r}) = e^{-i\mathbf{k}\cdot\mathbf{r}}\hat{\epsilon}_{\mathbf{k},j}$ is the spatial plane-wave mode. From Fourier analysis, we know that any spatial function can be decomposed as a linear combination of plane waves, since they constitute a complete basis in free-space. The orthogonality between two the modes, i.e. $\langle\mathbf{u}_{\mathbf{k},\hat{\epsilon}_{k,j}}|\mathbf{u}_{\mathbf{k'},\hat{\epsilon}_{k',j'}}\rangle = (2\pi)^2\delta^{jj'}\delta(\mathbf{k}-\mathbf{k'})$, is defined by the scalar product

$$\langle\mathbf{E}_\alpha(\mathbf{r})|\mathbf{E}_\beta(\mathbf{r})\rangle \equiv \iint_{z=cte} \mathrm{d}^2\mathbf{r}\ \mathbf{E}^*_\alpha(\mathbf{r})\cdot\mathbf{E}_\beta(\mathbf{r})\ , \tag{5}$$

where the mode overlap is evaluated at the plane perpendicular to the propagation direction (which we will take to be $\mathbf{z}$ without any loss of generality). The result of the overlap is independent from the plane $z = cte$ where the integral from Eq. (5) is evaluated. Note that two modes are orthogonal if their spatial parts are orthogonal.

Now imagine that we want to measure an incoming field. To do so, we collect the light with a lens and couple it to an optical fiber. The lens-fiber system allows certain spatial modes to be better transferred than the others. We call these privileged modes *detection modes*. Since the spatial parts and quantized amplitudes go together, only the ones shared between input and detection modes will have non-zero contribution due to orthogonality. This makes sense because to measure (annihilate) an excitation in one mode, we need the quantum operator acting on that specific mode.

3. The detection operator

With the tools from section 2, the next step is to obtain the total field operator associated to our specific case. Following the scheme described in section 1, our system has three fields: the pump, the probe and the one scattered by the atom. At any lens, our total field operator can be derived from the input-output relation [13, 17]

$$\hat{E}(\mathbf{r}) = \hat{E}_{in}(\mathbf{r}) + \mu_0 d_{eg}\omega_{ge}^2\mathbf{G}(\mathbf{r},\mathbf{r'},\omega_{eg})\cdot\mathbf{d}\ \hat{\sigma}^{ge}\ , \tag{6}$$

where the first term is the input field (the probe) and the second one is the field scattered by the atom in terms of the Green function $\mathbf{G}(\mathbf{r},\mathbf{r'},\omega_{eg})$. Here we do not write explicitly the annihilation operators to simplify the notation. However, formally, the total field operator $\hat{E}(\mathbf{r})$ acts on the infinite Hilbert space of the electromagnetic field modes tensor product the Hilbert space of the two-level atom (under the Born-Markov approximation). We already know that their spatial part can be decomposed in terms of plane-wave modes. Thus, we project the spatial parts of the operators from $\hat{E}(\mathbf{r})$ into a certain detection mode. The resulting field operator associated to the detection is

$$\hat{E}_{proj}(\mathbf{r}) = \hat{E}_{in,det}(\mathbf{r}) + \frac{id_{eg}k_0}{2\epsilon_0}\mathbf{E}^*_{det}(\mathbf{r}_d)\cdot\mathbf{d}\ \hat{\sigma}^{ge}\ , \tag{7}$$

where $\hat{E}_{in,det}(\mathbf{r})$ is the input field operator projected into a certain detection mode and $\mathbf{E}_{det}(\mathbf{r}_d)$ is the spatial part of the detection mode evaluated at the atom position. See Appendix B from the supplementary material for more details on how Eq. (7) is derived. In our case, we are interested in the fields collected at the probe lens, where only the probe and the scattered field are detected. For simplicity, let us assume that the detection mode coincides with the probe mode. The next step will be to obtain a more intuitive expression for Eq. (7) by connecting it to other physical quantities.

3.1. Connection between overlap and power

First, we notice that one can relate the self-overlap of a certain spatial mode with the electromagnetic power of the field. The energy per unit of time of a certain field can be obtained by integrating the z-component of its Pointing vector in the plane $z = 0$. From the definition of power flux (Eq. 2.56 [18]) and using Maxwell equations and Eq. (5), it is possible to define the power of an electromagnetic field as

$$P = 2\epsilon_0 c \int_{z=cte} \mathrm{d}^2\mathbf{r}\ \mathbf{E}^*(\mathbf{r}) \cdot \mathbf{E}(\mathbf{r}) = 2\epsilon_0 c\ \langle \mathbf{E}|\mathbf{E}\rangle\ . \tag{8}$$

3.2. Normalization of the projected total field operator

From Glauber's photo-detection theory [19], we know that the first-order auto-correlation function $G^{(1)}(0) = \langle \hat{E}^\dagger_{proj}\hat{E}_{proj}\rangle$ coincides with the counting rate of an ideal photo-detector. Then, it is convenient to re-normalize our fields to have $G^{(1)}(0)$ in units of photons per second. If one detects the light from an ideal source that emits entirely in the detection mode, the measured photon rate should be $\Phi_{det} = P_{det}/\hbar\omega$. Then:

$$\langle N\hat{E}^\dagger_{det}(\mathbf{r})N\hat{E}_{det}(\mathbf{r})\rangle = N^2|\langle \mathbf{E}_{det}|\mathbf{E}_{det}\rangle|^2 \equiv \Phi_{det} \rightarrow N = \frac{\sqrt{\Phi_{det}}}{|\langle \mathbf{E}_{det}|\mathbf{E}_{det}\rangle|}\ . \tag{9}$$

Since we assume the detection mode to be the probe mode, one could substitute one by the other in Eq. (9). From now on, any field operator will have this normalization.

3.3. Detection efficiency

The detection efficiency for the scattered field η is the ratio between the detected energy emitted by the dipole into the detection mode and the total emitted energy, i.e. $\hbar\omega_{eg}$. Additionally, the detected energy is the time integral of the power in the detection mode during the emission. Thus, considering the second term (associated to the scattered field) of the total field operator from Eq. (7) and the normalization Eq. (9),

$$\eta = \frac{1}{\hbar\omega}\int_0^\infty \mathrm{d}t\ |\hat{E}^{sc}_{proj}(t)|^2 = \frac{3\pi\Gamma_0}{2k_0^2|\langle \mathbf{E}_p|\mathbf{E}_p\rangle|}|\mathbf{E}_p(\mathbf{r}_d)\cdot\mathbf{d}|^2\int_0^\infty \mathrm{d}t\ \hat{\sigma}^{ee}(t)\ . \tag{10}$$

If the atom starts in the excited state, the population decays exponentially at a rate Γ_0 so that

$$\eta = \frac{3\pi}{2k_0^2}\frac{|\mathbf{E}_p(\mathbf{r}_d)\cdot\mathbf{d}|^2}{|\langle \mathbf{E}_p|\mathbf{E}_p\rangle|} \approx \frac{3}{8\pi^2}\frac{\lambda^2}{w_0^2}\ , \tag{11}$$

where, to give a more intuitive result, we have substituted the values for the particular case of a paraxial, Gaussian probe field with beam waist w_0. Putting everything together, we start from Eq. (7), introduce the normalization from Eq. (9) and substitute the detection efficiency from Eq. (11) to obtain

$$\hat{E}_{proj} = \hat{E}_{in,p} + i\sqrt{\eta\Gamma_0}\,\hat{\sigma}^{ge} \approx \hat{E}_{in,p} + i\sqrt{\frac{3\Gamma_0}{8\pi^2}}\frac{\lambda}{w_0}\hat{\sigma}^{ge}\ . \tag{12}$$

The normalization is such that $\langle \hat{E}^{\dagger}_{in,p}\hat{E}_{in,p}\rangle$ is the input photon flux projected into the probe mode Φ_p. Let us check if the previous result makes sense. Computing the expected value of the first term modulus squared, we get the number of photons per second detected from the probe, i.e. Φ_p. Since the probe is the detection mode, any input probe photon gets detected. Doing the same for the second term, we get $\eta\Gamma_0\langle\hat{\sigma}^{ee}\rangle$, i.e. the photon flux measured from the scattered field into the detection mode.

4. Glauber correlation functions with the projected field operator

Once the operator associated to the detection has been established, the first and second-order auto-correlation functions associated to the operator from Eq. (7) are [19]

$$G^{(1)}(0) = \langle \hat{E}^{\dagger}_{in,p}\hat{E}_{in,p}\rangle + 2\sqrt{\eta\Gamma_0}\,\mathbb{R}\{i\langle\hat{\sigma}^{ge}\hat{E}^{\dagger}_{in,p}\rangle\} + \eta\Gamma_0\langle\hat{\sigma}^{ee}\rangle\ , \tag{13}$$

$$G^{(2)}(0) = \langle \hat{E}^{\dagger}_{in,p}\hat{E}_{in,p}\rangle\left[\langle \hat{E}^{\dagger}_{in,p}\hat{E}_{in,p}\rangle + 4\sqrt{\eta\Gamma_0}\,\mathbb{R}\{i\langle\hat{\sigma}^{ge}\hat{E}^{\dagger}_{in,p}\rangle\} + 4\eta\Gamma_0\langle\hat{\sigma}^{ee}\rangle\right]\ , \tag{14}$$

where $\langle \hat{E}^{\dagger}_{in,p}\hat{E}_{in,p}\rangle = \Phi_p$. However, to discuss the statistical properties of the photon correlations in a quantitative way, we need to compute the normalized version of the correlation functions. We will only focus on the normalized second-order auto-correlation function defined as $g^{(2)} = G^{(2)}(0)/|G^{(1)}(0)|^2$. Since the resulting expression is quite dense, we would like to give a much more intuitive result. Thus, let us work the following particular case.

4.1. Particular case: paraxial, Gaussian probe field

To simplify things out, let us assume that the input probe field is a paraxial, Gaussian field. Second, we notice that the input field and the scattered one are not independent from each other. If we increase the input photon flux, the scattered flux will also increase. The final results for the $g^{(2)}(0)$ will depend on the ratio between these two fluxes, so it is convenient to know beforehand its value. In general, the parameter that relates them is what we call the scattering ratio (or scattering probability) R_{sc}. Imagine that we illuminate our atom with a single probe field (no pump) with photon flux Φ_p. Then, the atom will scatter $R_{sc}\Phi_p$ photons per second. At the same time, the photon flux scattered by the atom is $\Gamma_0\rho^{ee}_{probe}$ where, in the weak driving regime, $\rho^{ee}_{probe} \sim \Omega_p^2/\Gamma_0^2$. Thus, we can establish the relation $R_{sc}\Phi_p = \Gamma_0\rho^{ee}_{probe}$.

If we add a pump beam, the previous relation is still valid in the linear regime. However, the total scattered flux is now $\Gamma_0\rho^{ee}$, where ρ^{ee} is then associated to a global

Rabi frequency Ω. Here we have $\Omega = \Omega_p + \Omega_P$, where Ω_p is the contribution from the probe and Ω_P is the one from the pump. With all this, we can relate the probe photon flux to the total scattered photon flux (with the pump illuminating) through

$$\frac{\Phi_{atom}}{\Phi_p} = \frac{(\Gamma_0 \rho^{ee})}{\left(\frac{\Gamma_0 \rho^{ee}_{probe}}{R_{sc}}\right)} = R_{sc} \frac{|\Omega|^2}{|\Omega_p|^2} \ . \tag{15}$$

Finally, combining Eq. (13), Eq. (14), the definition of the $g^{(2)}(0)$, dividing everything by Φ_p^2 to use Eq. (15), assuming that we have a paraxial, Gaussian probe field and working in the weak driving regime we get:

$$g^{(2)} = \frac{G^{(2)}(0)}{|G^{(1)}(0)|^2} \approx \frac{1 - 4\frac{3}{8\pi^2}\frac{\lambda^2}{w_0^2}\mathbb{R}\left\{\frac{\Omega}{\Omega_p}\right\} + 4\frac{3^2}{8^2\pi^4}\frac{\lambda^4}{w_0^4}\left|\frac{\Omega}{\Omega_p}\right|^2}{\left|1 - 2\frac{3}{8\pi^2}\frac{\lambda^2}{w_0^2}\mathbb{R}\left\{\frac{\Omega}{\Omega_p}\right\} + \frac{3^2}{8^2\pi^4}\frac{\lambda^4}{w_0^2}\left|\frac{\Omega}{\Omega_p}\right|^2\right|^2} \ , \tag{16}$$

which depends exclusively on the probe beam waist w_0 and the Rabi frequencies Ω_p and Ω_P respective to each one of the input beams. Here we are free to take the probe beam in phase with the dipole matrix element such that Ω_p is real. Then, if the pump has a certain relative phase with respect to the probe, Ω_P becomes complex. From Eq. (16) it is possible to find conditions for the total bunching ($G^{(1)}(0) \to 0, g^{(2)}(0) \to \infty$) and anti-bunching ($G^{(2)}(0) \to 0, g^{(2)}(0) \to 0$) such that

$$\text{Bunching when } \frac{8\pi^2 w_0^2}{3\lambda^2} = \frac{\Omega}{\Omega_p} \ , \qquad \text{Anti-bunching when } \frac{4\pi^2 w_0^2}{3\lambda^2} = \frac{\Omega}{\Omega_p} \ , \tag{17}$$

which are valid for $\Omega \in \mathbb{R}$, i.e. the pump and the probe having equal phase. This result agrees with what we discussed in section 1. To have relevant photon correlations due to the interference between scattered and input fields, we need them to have comparable strengths. Since the scattered field contribution is in general smaller, we introduce a pump beam that compensates for the low scattering probability and detection efficiency. This tells us that for an arbitrary focusing of the input fields, one can find a pump/probe ratio such that relevant features in the $g^{(2)}(0)$ can be observed. For the equations to hold, one has to ensure $\Omega \ll \Gamma_0$ for the weak driving approximation to be valid. This could set a practical limit, in the sense that, for very bad focusing, the required attenuation in the probe is so large that few events are registered among large periods of time. However, this constitutes a novel approach to obtain interesting photon statistics with single atoms in free space without diffraction-limited focusing.

To give some numerical values, we simulate the $g^{(2)}(0)$ from the light collected at the probe lens. In Figure 3(a), large bunching and anti-bunching are observed for a particular w_0 when Ω is close to real (relative phase between pump and probe is zero, $\phi = 0$). Additionally, in Figure 3(b) we show that the Rabi frequency is inversely proportional to w_0^2/λ^2 when bunching appears, as predicted from Eq. (17). Therefore, as long as the beam waist is not much larger than the wavelength, we can find a pump intensity to satisfy Eq. (17) within the weak driving approximation.

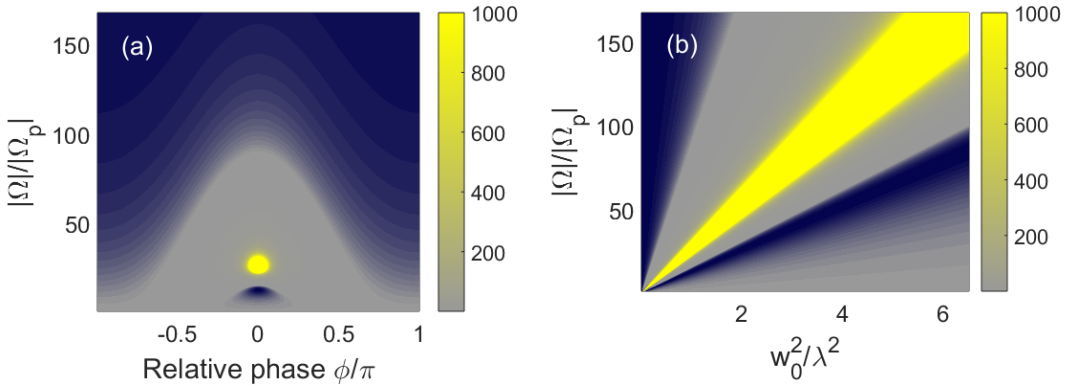

Figure 3: Plots of the second-order auto-correlation function. In (a) we set the probe beam waist to $w = \lambda$ and change the relative phase and amplitude between pump and probe. In (b) we set the phases of pump and probe to be equal and change the pump/probe amplitude ratio and the probe beam waist. The color code is the usual: yellow for bunching and blue for anti-bunching. We truncate at $g^{(2)}(0) < 10^3$.

Finally, we would like to give more arguments in favor of the presented results. To give some intuition on the origin of these effects (specially in the bunching case), let us study the atomic state after the measurement of a photon at the detector.

4.2. State after the mode-projecting measurement

Let us consider the initial atomic state $|\Psi\rangle = |g\rangle + \alpha|e\rangle$, where $|\alpha|$ is very small (since we are in the weak driving regime). The parameter α can be obtained from $\alpha = \langle\hat{\sigma}^{ge}\rangle = i\Omega/\Gamma_0$ because $\langle\Psi|\hat{\sigma}^{ge}|\Psi\rangle = \alpha$. Intuitively, the measurement of a photon from the collected field will project the atom into a certain atomic state. We use the mode-projected field operator from Eq. (12), which we know that also acts on the atomic Hilbert space. To express the normalized, final state, it is more convenient to use the Bloch Sphere representation. In that framework, the transient state after the measurement is $|\Psi'\rangle \equiv \cos(\theta/2)|g\rangle + \sin(\theta/2)e^{i\gamma}|e\rangle$, where θ satisfies

$$\tan(\theta/2) = \frac{\left|\sqrt{\Phi_p}\frac{\Omega}{\Gamma_0}\right|}{\left|\sqrt{\Phi_p} - \sqrt{\eta\Gamma_0}\frac{\Omega}{\Gamma_0}\right|} = \frac{\sqrt{\Phi_p}}{\sqrt{G^{(1)}(0)}}\frac{|\Omega|}{\Gamma_0} \,. \tag{18}$$

Here we have identified the $G^{(1)}(0)$ from Eq. (13) in the weak driving regime. From Eq. (18), the atom is projected into the ground state when $\tan(\theta/2) = 0$. This occurs for $\Omega = 0$ (when the atom is not being driven at all) or for $\Phi_p = 0$ (only the scattered photons can be measured, projecting always the atom into the ground state). On the other hand, again from Eq. (18), the excited state is obtained when the $G^{(1)}(0)$ is cancelled, which occurs when the bunching condition from Eq. (17) is fulfilled. This suggests the connection $|\Phi'\rangle \to |e\rangle \iff G^{(1)}(0) \to 0$.

To justify this, let us consider the case where the system is close to meet the bunching condition. Since the pump field compensates for the low scattering rate and detection efficiency, the probe field can be effectively cancelled by the enhanced,

projected scattered field. Since it is unlikely to measure input field photons or photons scattered linearly by the atom, this opens a window to measure photons from non-linear processes, like frequency mixing. In these cases, the atom transforms two resonant input photons into two photons with frequencies $\omega_{eg} \pm \Omega$. This is usually depicted as the side-peaks of the Mollow triplet in the two-level atom emission spectra. The shift in frequency prevents them from being cancelled by the resonant input field‡. Therefore, we are left with only the photons from non-linear processes, which are the ones detected.

From Eq. (18), the measurement of a single-photon when close to the total bunching condition ($G^{(1)}(0) \approx 0$) projects the atom into a transient state in which it is mostly inverted. This has to be understood as the atom being very likeable to emit a second photon, completing the two-photon process. The scattered photons become highly correlated as it is not possible to measure independent ones (linear processes are cancelled). With all this, we identify the connection between the projection into the excited state and the bunching condition. In Figure 4, we plot the population in the excited state after the measurement of a photon. By comparing Figures 4(a) with 3(a) and Figures 4(b) with 3(b), one explicitly sees the previous connection.

Similar arguments can be used to justify the anti-bunching case. In that case, we need to study the state after the measurement of one and two photons. When the anti-bunching condition is close to being fulfilled, the probability to detect the first photon is relatively high. However, the detection of the second photon is very unlikable, because the field of the second photon is very weak (second-order processes are suppressed by the input field). Thus, in the majority of events, one gets the detection of a single photon which justifies the anti-bunching.

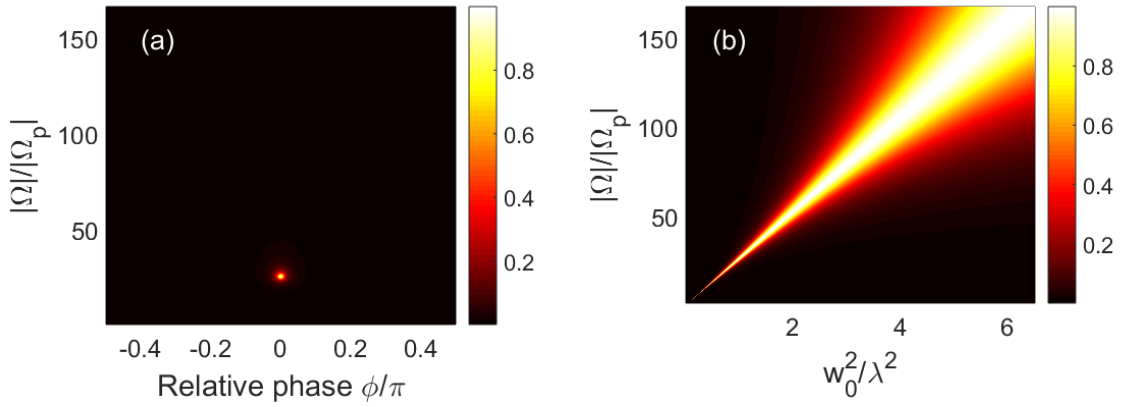

Figure 4: Population in the excited state of the atom after the measurement of a photon. In (a) we fix the beam waist of the probe field to $w_0 = \lambda$ and study the $g^{(2)}(0)$ and the population in the excited state as a function of $|\Omega|/|\Omega_p|$ and the relative phase between pump and probe. In (b) we do the same but now fixing the relative phase between pump and probe to zero and explore different probe waists.

‡ As it can be seen in the Appendix B, the scattered field part of Eq. (7) contains a combination of annihilation operators in different frequencies that covers the atomic emission spectra. Thus, the non-linear photons can also be measured by the operator associated to the detection from Eq. (12).

5. Conclusions

We have presented a novel approach to calculate and engineer the photon correlations emerging from the interference between an input field and the field scattered by an atom in free space. Without requiring a diffraction-limited focusing, large bunching and total anti-bunching could be found with a proper tunning of the pump and probe (as long as the weak driving approximation holds).

Additionally, we have seen a physical justification for the non-trivial photon correlations to appear. When the system is close to the total bunching condition, the linear scattered field is suppressed by the input field. The probability of detecting the first photon is very low, since the total field is weak ($G^{(1)}(0) \approx 0$). However, once it is detected, it is always followed by a second photon. This is so because we are left with second-order processes, the photons of which are intrinsically bunched. There is a similar connection between anti-bunching and the suppression of second-order processes.

6. Acknowledgements

I would like to thank the whole Theoretical Quantum Nano-Photonics group for giving me support and guidance, specially to Prof. Darrick Chang and Dr. Mariona Moreno for all their thoughtful advice.

References

[1] C. Schuck *et. al.* (2010), *Phys. Rev. A* **81**, 011802(R).
[2] J. I. Cirac, P. Zoller, H. J. Kimble, H. Mabuchi (1997) *Phys. Rev. Lett.* **78** 3221.
[3] L. M. Duan , M. D. Lukin , J. I. Cirac and P. Zoller (2001) *Nature* **414** 6862.
[4] J. D. Thompson *et. al.* (2008) *Nature* **452** 7183.
[5] A. B. Mundt *et. al.* (2002) *Phys. Rev. Let.* **89** 103001.
[6] R. J. Bettles, S. A. Gardiner and C. S. Adams (2016) *Phys. Rev. Lett.* **116** 103602.
[7] J. T. Shen. S. Fan. (2007) *Phys. Rev. Let.* **98** 153003.
[8] M. K. Tey (2009) *New J. of Phys.* **11** 043011.
[9] G. Leuchs, M. Sondermannb (2013) *J. Mod. Opt.* **60** 136-42.
[10] Y. S. Chin, M. Steiner, C. Kurtsiefer (2017) *Nature Communications* **8**, 1200.
[11] S. J. Van Enk, H. J. Kimble (2000) *Phys. Rev. A* **61** 051802(R).
[12] N. Bruno *et. al.* (2019) arXiv:1902.03220.
[13] H. T. Dung, L. Knoll, D. G. Welsch (2002) *Phys. Rev. A* **66** 063810.
[14] A. Asenjo-Garcia, J. D. Hood, D. E. Chang, H. J. Kimble (2017) *Phys. Rev. A* **95** 033818.
[15] D. A. Steck, *'Quantum and Atom Optics'* (2019) available online at Link.
[16] P.S. Venkataram, *'Electromagnetic Field Quantization'*, MIT Department of Physics, class notes 8.06 (2013) available online at Link.
[17] M. T. Manzoni *et. al.* (2018) New J. Phys. **20** 083048.
[18] L. Novotny, B. Hecht, (2012) *'Principles of Nano-optics'*, Cambridge University Press, p. 24.
[19] R. J. Glauber (1963) *Phys. Rev. A* **130** 2529.